Chemical Engineering Journal xxx (xxxx) xxx

Contents lists available at ScienceDirect

Chemical Engineering Journal

journal homepage: www.elsevier.com/locate/cej

CTAB-controlled synthesis of phenolic resin-based nanofiber aerogels for highly efficient and reversible SO_2 capture

Zhang-Min Li [a], Shu-Xian Zhu [a], Fei-Feng Mao [a], Yan Zhou [a], Wenshuai Zhu [b], Duan-Jian Tao [a,*]

[a] Key Laboratory of Functional Small Molecules for Ministry of Education, College of Chemistry and Chemical Engineering, Jiangxi Normal University, Nanchang 330022, PR China
[b] School of Chemistry and Chemical Engineering, Institute for Energy Research, Jiangsu University, Zhenjiang 212013, PR China

ARTICLE INFO

Keywords:
Aerogels
Nanofiber
Sulfur dioxide
Adsorption capacity
Selectivity

ABSTRACT

Currently available aerogels as effective adsorption materials for capture of trace sulfur dioxide (SO_2) are unfavorable from the perspective of deep desulfurization technologies. Herein, four phenolic resin-based aerogels with controlled structures varying from spherical (~1 μm) to nanofiber (~20 nm) were prepared and characterized using hexadecyl trimethyl ammonium bromide (CATB) as a soft template. It is demonstrated that adjusting the usage amount of CTAB from 0.00 to 0.15 g could effectively regulate SO_2 adsorption capacities of phenolic resin-based aerogels. AG-0.15 nanofiber aerogel exhibited an outstanding SO_2 uptake through a swelling mechanism (10.58 mmol g^{-1} at 298.2 K, 1.0 bar), and displayed a very high SO_2/N_2 selectivity (7271 at 298.2 K). Moreover, AG-0.15 nanofiber aerogel also had excellent performance for selective capture of 2000 ppm SO_2 in the mixed $SO_2/N_2/CO_2$ gases through dynamic column breakthrough experiments. Overall, phenolic resin-based nanofiber aerogels are perceived as a promising adsorbent for effective removal of trace SO_2 from flue gas.

1. Introduction

The emission of sulfur dioxide (SO_2) mainly comes from many tail gases including coal-fired power plants, heavy oils and metallurgical processes, which is a significant risk for human health and increasing environmental burdens [1–4]. The capture and removal of SO_2 through a limestone scrubbing process is proved to be an effective technology for flue gas desulfurization, but the deal and utilization of gypsum waste remains an open question [5,6]. To meet the green development of society and industry, selective adsorption and removal of SO_2 from flue gas by solid adsorption have received a lot of attention. This adsorption separation technology can take the advantage of low investment of equipment, easy regeneration of solid adsorbent, and low consumption of energy. Therefore, it is highly desirable to screen the adsorbent materials with both large SO_2 capacity and excellent selectivity.

Up to now, various porous materials including zeolites [7,8], metal–organic frameworks (MOFs) [9], activated porous carbon [10,11], and covalent organic polymers [12] have been reported and developed for SO_2 capture through adsorption separation technology. For example, Yang and his co-workers [13] prepared a robust Zn-based MOF material for SO_2 capture and achieved the SO_2 adsorption capacity of 12.3 mmol g^{-1} at 298.2 K and 1.0 bar. An et al. [14] also prepared a kind of hollow nanotube ionic polymer for rapid SO_2 capture with an uptake capacity of 7.2 mmol g^{-1} at 298.2 K and 1.0 bar. In view of this, owing to the unique characteristics of tunable structure and morphology, aerogels have promising applications in acidic gas capture [15–17]. Compared with other types of adsorbent materials, aerogels also have many unique advantages such as low density, adjustable surface chemistry, and versatile properties through sol–gel process [18]. So far, inorganic aerogels, organic aerogels, and hybrid aerogels have been reported for highly efficient capture of CO_2 [19–22]. However, the adsorption efficiency of SO_2 in currently available aerogels is not good as the case of CO_2 capture [23–25]. As well known, SO_2 is always coexisting with the competitive gas CO_2. SO_2 molecular shows more acidity than CO_2, indicating that the less basicity of adsorbent materials would be in favor of SO_2 capture. Also, many adsorbent materials possessing the characteristics of very large surface area and high porosity would result in a certain amount of N_2 and CO_2 uptake capacities, which is hard to achieve good separation performance of $SO_2/CO_2/N_2$ mixture. Therefore, it is worthwhile but challenging to design and synthesize new aerogels with high SO_2 adsorption capacity and low competing gas uptake capacity.

Herein, four phenolic resin-based aerogels with controllable

* Corresponding author.
E-mail address: djtao@jxnu.edu.cn (D.-J. Tao).

https://doi.org/10.1016/j.cej.2021.133715
Received 7 October 2021; Received in revised form 14 November 2021; Accepted 15 November 2021
Available online 20 November 2021
1385-8947/

structure and morphology were prepared by polymerization of 3-aminophenol and hexamethylenetetramine using hexadecyl trimethyl ammonium bromide (CTAB) as a soft template. Then many characterization technologies were used for confirming the structure of these phenolic resin-based aerogels. By tuning the usage amount of CTAB, the morphology and particle size of phenolic resin-based aerogels (donated as AG-*x*, *x* is the usage amount of CTAB) could be precisely regulated, and AG-0.15 nanofiber aerogel could be as superior adsorbents for highly efficient and reversible SO_2 capture. In addition, the excellent performance of AG-0.15 nanofiber aerogel for efficient removal of 2000 ppm SO_2 in the mixed $SO_2/N_2/CO_2$ gases was further verified via column breakthrough experiments at 298.2 K and 1.0 bar.

2. Experimental

2.1. Materials

Gases including CO_2 (99.99 vol%), SO_2 (99.99 vol%), N_2 (99.99 vol %) and He (99.99 vol%) were provided by Jiangxi Huate Special Gas Co., Ltd. Chemicals including 3-Aminophenol (98%), hexamethylenetetramine (HMTA, 99%), and hexadecyl trimethyl ammonium bromide (CTAB, 90%) were supplied from Shanghai Aladdin Biochemical Co., Ltd. All chemicals were used as received without further purification.

2.2. Synthesis of phenolic resin aerogel

Scheme 1 demonstrates the CTAB-controlled synthesis of phenolic resin-based aerogels via a condensation polymerization of 3-aminophenol and HMTA with different usage amounts of CTAB. Typically, 3-aminophenol (0.2 g) and HMTA (0.514 g) were dissolved in deionized water (20 mL). 0.15 g CTAB was then added to the solution. After stirring at 298.2 K for 20 min, the mixture was heated at 358.2 K for 24 h under N_2 atmosphere to obtain the hydrogel. By freeze-drying treatment of hydrogel, a light powder was obtained and washed at least three times with deionized water. After that, AG-0.15 nanofiber aerogel was thus obtained by drying the solid powder at 353.2 K for 12 h. Similarly, AG-0.00, AG-0.05, and AG-0.10 aerogels were prepared according to the procedure except for 0.00 g, 0.05 g, and 0.10 g CTAB, respectively.

2.3. Characterization methods

The morphology of phenolic resin-based aerogels was characterized by field emission scanning electron microscope (SEM, HITACHI SU8020) and transmission electron microscopy (TEM, JEOL JEM-2100). N_2 adsorption–desorption data were tested by Micromeritics TriStar II 3020 at 77 K. CO_2 and N_2 adsorption experiments were also measured by Micromeritics TriStar II 3020 at 298.2 K. The thermal analysis was performed by the PerkinElmer Diamond TG/DTA apparatus. The surface elemental chemical composition was recorded on AXIS Supra X-ray photoelectron spectroscopy (XPS, Kratos Analytical), equipped with an Al Kα radiation source. Fourier transform infrared (FTIR) spectra were measured by a Nicolet 6700 spectrometer. X-ray diffraction (XRD) data was carried out on a Bruker D8 ADVANCE diffractometer. The temperature programmed desorption of CO_2 (CO_2-TPD) was performed on a VDsorb-91i chemisorption instrument.

2.4. SO_2 adsorption procedure

The apparatus for capturing SO_2 is the same as our previous work (Fig. S1, Supplementary data) [26,27]. Briefly, in a typical adsorption process of SO_2, a known mass of aerogels was put into adsorption chamber. Partial SO_2 was introduced into the adsorption chamber. Adsorption data were recorded until after the achievement of equilibrium. The ideal adsorption solution theory (IAST) selectivity of SO_2/CO_2 and SO_2/N_2 in pure gas was then measured according to the model equation presented by Myers et al [28,29]. For regeneration, the SO_2-saturated aerogels were maintained at 348.2 K for 2 h under vacuum to release SO_2 and then the recycled aerogels were reused for the next run. In addition, the dynamic breakthrough experiments for 2000 ppm SO_2 in the mixed $SO_2/CO_2/N_2$ gases were conducted using a homemade apparatus, as shown in Fig. S2 in the Supplementary data.

3. Results and discussion

3.1. Characterization of phenolic resin-based aerogels

Fig. 1A shows the XRD pattern of these four phenolic resin-based aerogels. It is found that there is a broaden peak at around $2\theta = 22^\circ$, indicating the patterns of amorphous features in these phenolic resin-based aerogels. Fig. 1B illustrates the FTIR spectra of these four phenolic resin-based aerogels. The characteristic peaks at 3425, 2923, and 1622 cm^{-1} were discovered and assigned to the –OH group, $–CH_2$ group, and C = C bond on the aryl group, respectively [30,31]. This indicates that the condensation polymerization has successfully

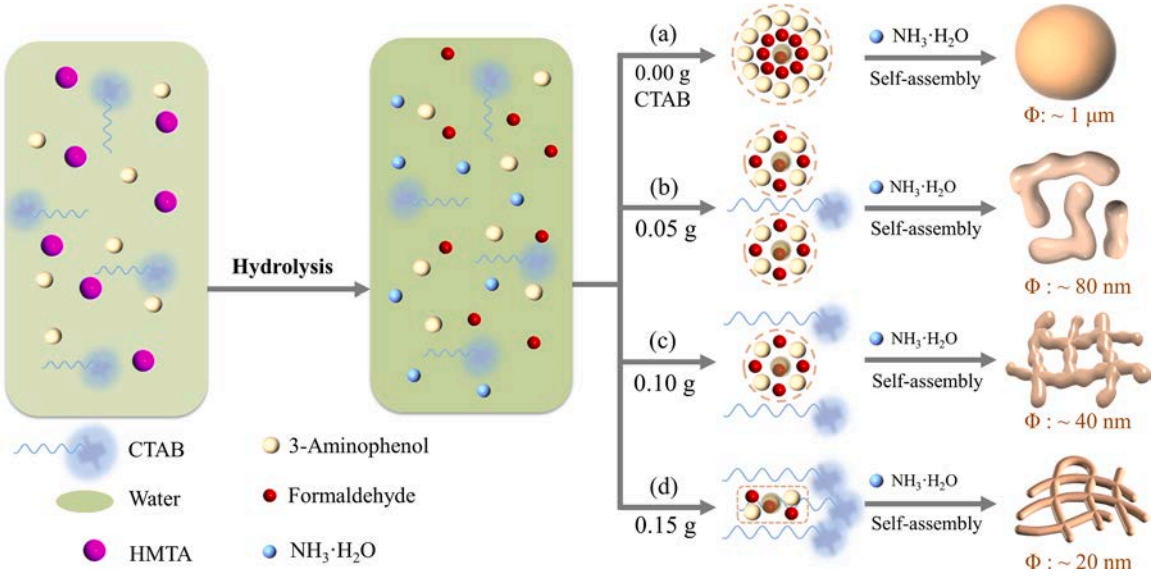

Scheme 1. Schematic diagram for preparation of phenolic resin-based aerogels with controlled morphologies and sizes using CATB as a soft template.

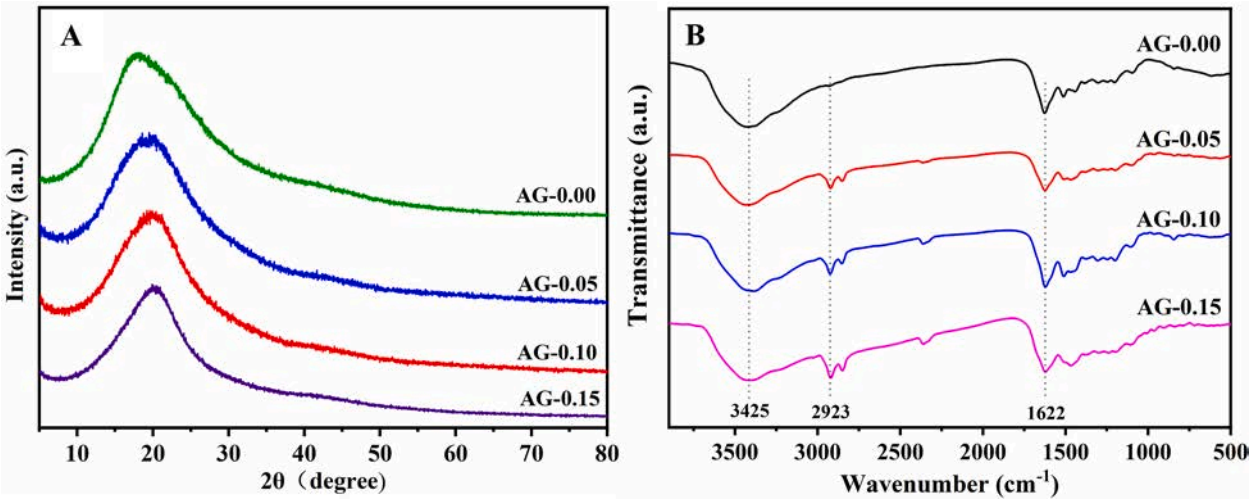

Fig. 1. XRD patterns (A) and FTIR spectra (B) of four phenolic resin-based aerogels.

occurred between 3-aminophenol and formaldehyde formed by hydrolysis of hexamethylenetetramine. The thermal stability of these four phenolic resin-based aerogels was also examined (Fig. S3, Supplementary data). It is found that all the phenolic resin-based aerogels were sufficiently stable up to 473 K. The adsorption temperature of up to 338.2 K and the desorption temperature of 353.2 K cannot destroy the structure of phenolic resin-based aerogels, which ensures the stability of phenolic resin aerogel during SO_2 adsorption–desorption recycles.

The structure and morphology of these four phenolic resin-based aerogels were characterized by SEM (Fig. 2) and TEM (Fig. 3). It is found that all the four phenolic resin-based aerogels showed dense structures and the usage amount of CTAB had a significant impact on the control of particle size and morphology of phenolic resin-based aerogels. Then the schematic for CTAB-controlled synthesis of four kinds of phenolic resin-based aerogels was illustrated in Scheme 1. Without using CTAB, a well-defined spherical shape and uniform diameter of ~ 1 μm particles were formed and obtained in AG-0.00 aerogel (Fig. 2A,3A). When the usage amount of CTAB was 0.05 g, AG-0.05 aerogel had a short spherical chain structure with a diameter of ~ 80 nm (Fig. 2B,3B). With a further increase to 0.15 g CTAB, the spherical particles were disappeared and AG-0.15 aerogel exhibited a noodle-like nanofiber structure with a diameter of ~ 20 nm (Fig. 2D,3D). These observations demonstrate that the particle size of phenolic resin-based aerogels reduces with the increase of CTAB amount. Adjusting the amount of CATB

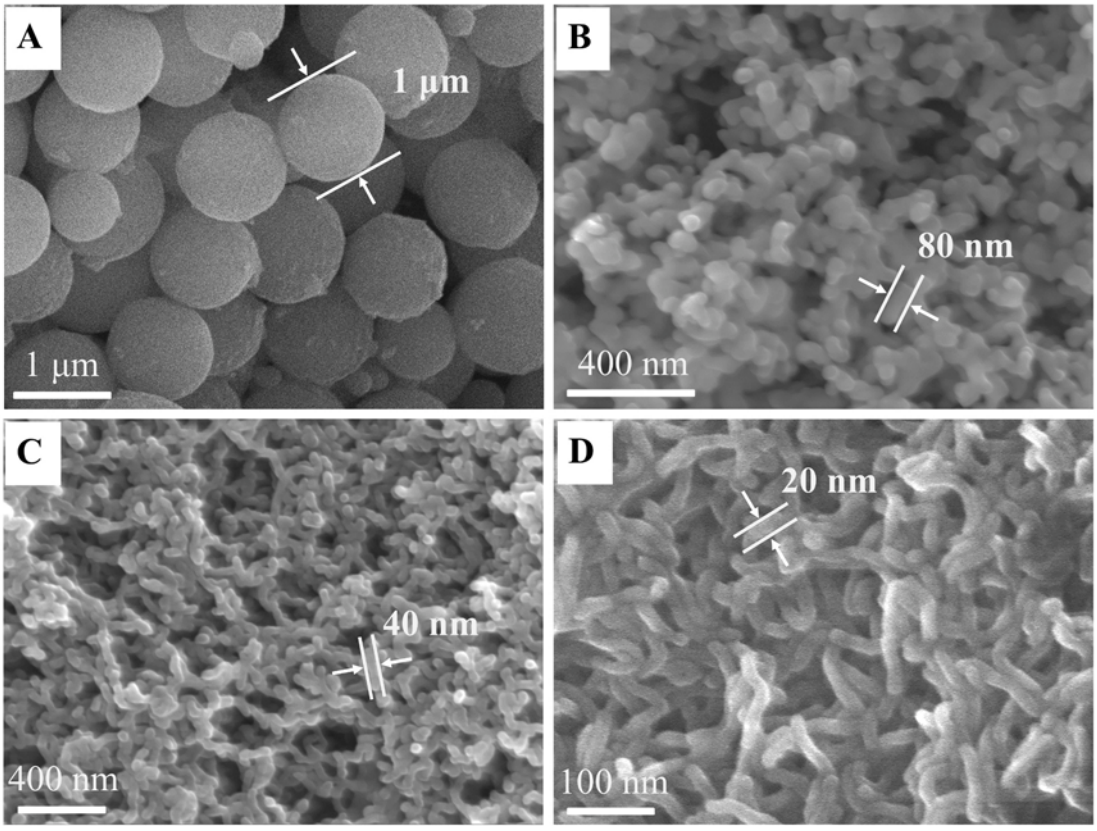

Fig. 2. SEM images of four phenolic resin-based aerogels: (A) AG-0.00; (B) AG-0.05; (C) AG-0.10; (D) AG-0.15.

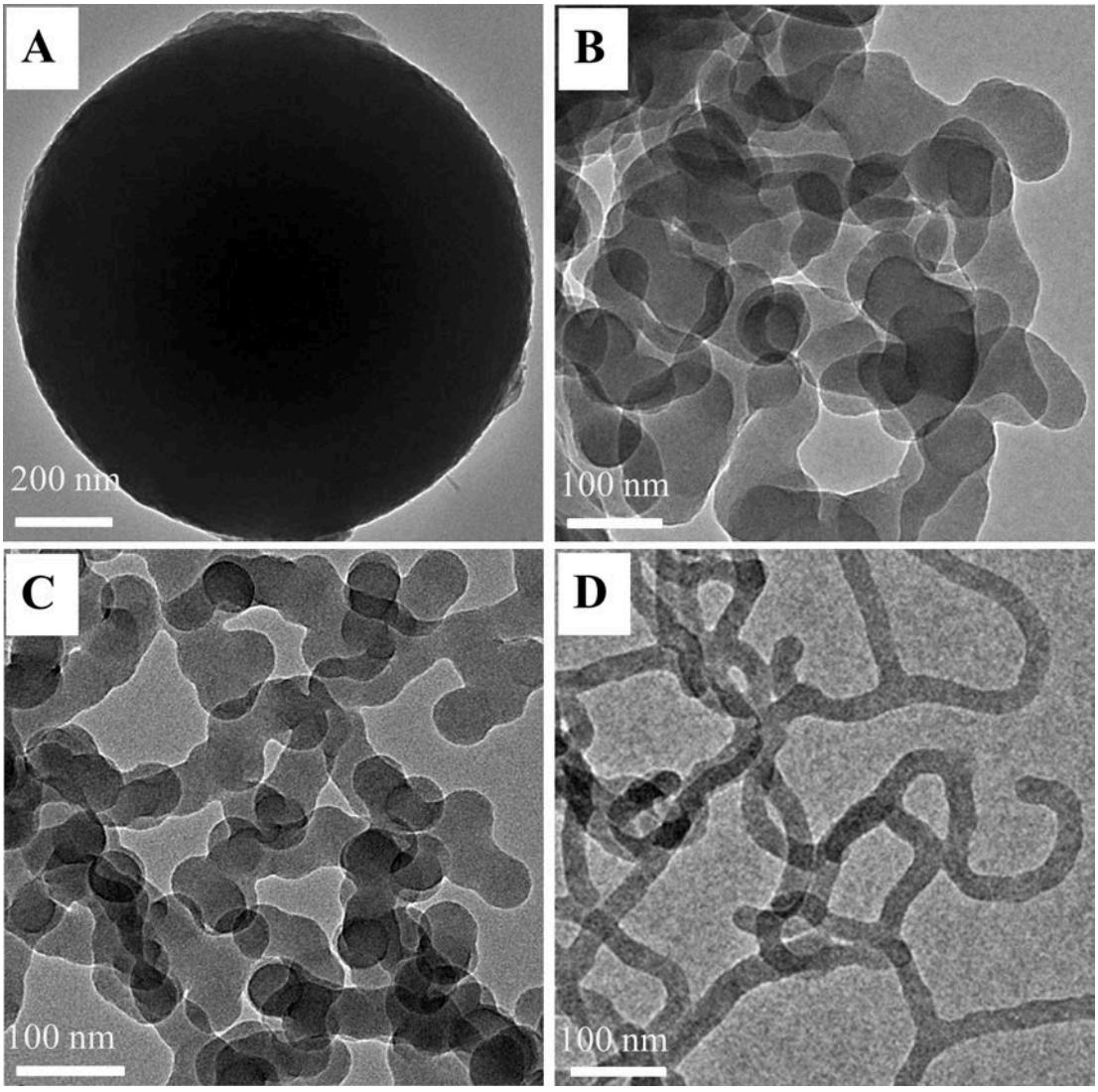

Fig. 3. TEM images of four phenolic resin-based aerogels: (A) AG-0.00; (B) AG-0.05; (C) AG-0.10; (D) AG-0.15.

can effectively control and regulate the structure and morphology of phenolic resin-based aerogels.

The porosities and surface areas of these four phenolic resin-based aerogels were further determined by N_2 adsorption/desorption at 77 K. It is found that AG-0.00 aerogels displayed a very low N_2 adsorption capacity and had a very small surface area (Fig. 4). In contrast, the other three phenolic resin-based aerogels (AG-0.05, AG-0.10, and AG-0.15) exhibited type-II isotherms with a H3 hysteresis loop at 0.9 ~ 1.0P/P_0. Their surface areas were around 50 ~ 85 $m^2\ g^{-1}$. This suggests that many slit-shaped pores are existed in AG-0.05, AG-0.10, and AG-0.15 aerogels, which are formed by the aggregation and stack of dense spherical or nanofiber particles [32]. Notably, increasing the usage amount of CTAB can result in a relatively large surface area and small particles size of phenolic resin-based aerogels.

The XPS characterization for phenolic resin-based aerogels was further performed. The C, N, O, and Br elements can be clearly observed in the full-scan spectra of four phenolic resin-based aerogels, as shown in Fig. S4A in the Supplementary data. The N 1 s XPS spectra of these four phenolic resin-based aerogels can be deconvoluted to three peaks at 399.3, 400.7, and 402.7 eV (Fig. 5), which corresponds to tertiary N, secondary N, and quaternary N, respectively. Moreover, it is notable that increasing the amount of CTAB could enhance the binding energy of tertiary N but reduce the binding energy of Br^- in phenolic resin-based

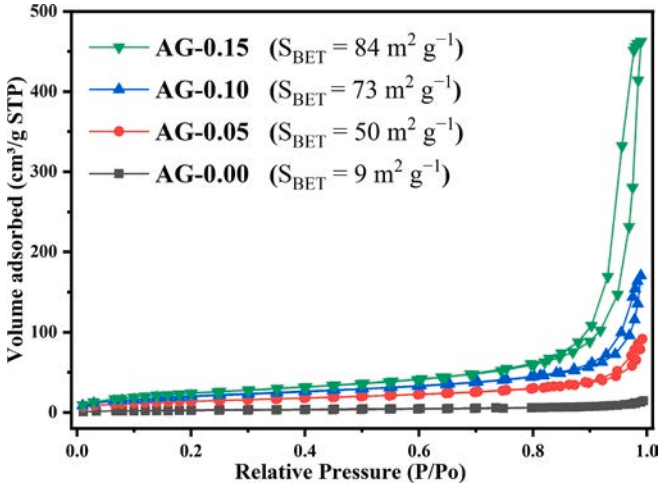

Fig. 4. N_2 adsorption/desorption isotherms of four phenolic resin-based aerogels.

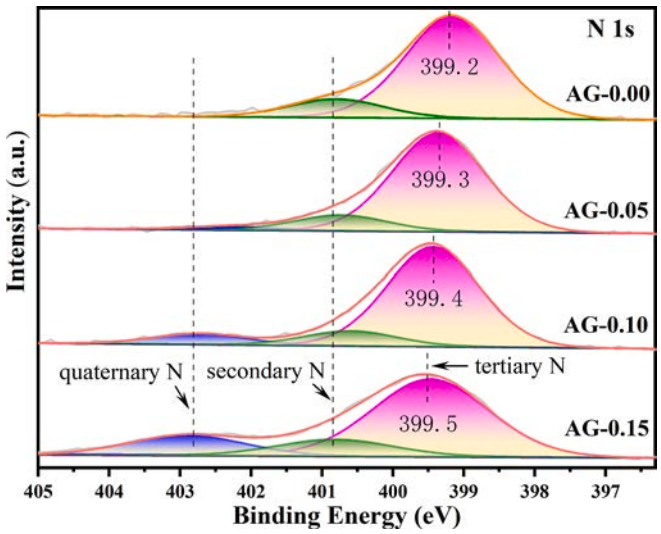

Fig. 5. The N 1 s XPS spectra of four phenolic resin-based aerogels.

aerogels. For example, the binding energy of tertiary N in the AG-0.10 aerogel was only 399.4 eV, while the usage amount of 0.15 g CTAB resulted in the binding energy of tertiary N at 399.5 eV in AG-0.15 nanofiber aerogel. Meanwhile, compare to AG-0.10, the binding energies of Br 3d ($3d_{5/2}$ and $3d_{3/2}$) in AG-0.15 nanofiber aerogel decreased from 67.8 and 68.8 eV to 67.6 and 68.7 eV, respectively [33] (Fig. S4B, Supplementary data). Additionally, the larger binding energy of tertiary N means less electron cloud density on the N element and leads to the weaker Lewis basicity. Thus, the above-mentioned results show that compared with the other three phenolic resin-based aerogels, the interaction between AG-0.15 nanofiber aerogel and SO_2 would be not strong because of the relatively weak basicity of AG-0.15 nanofiber aerogel. This would facilitate the effortless desorption of adsorpted SO_2 from AG-0.15 nanofiber aerogel and regeneration and reuse of AG-0.15 nanofiber aerogel.

3.2. SO_2 adsorption performance

The performance of phenolic resin-based aerogels for the adsorption of pure SO_2 gas was investigated at 298.2 K and 1.0 bar. As shown in Table 1, these four phenolic resin-based aerogels exhibited different SO_2 adsorption capacities, and the sequence was AG-0.15 > AG-0.10 > AG-0.05 > AG-0.00. This means that the uptake capacity of SO_2 is closely associated with the surface area of phenolic resin-based aerogels. Owing to the largest usage amount of 0.15 g CTAB, AG-0.15 nanofiber aerogel had the smallest particle size (~20 nm) and exhibited the highest surface area of 84 $m^2\ g^{-1}$. This implies that AG-0.15 nanofiber aerogel would have the best exposure of active sites in participating SO_2 adsorption and thereby leads to the largest SO_2 uptake capacity of 10.58 mmol g^{-1} at 298.2 K and 1.0 bar. Moreover, AG-0.15 nanofiber aerogel could have the SO_2 uptake of 1.43 mmol g^{-1} even at an extremely low pressure of 0.01 bar. Thus, it is demonstrated that AG-0.15 nanofiber aerogel displayed an excellent SO_2 uptake capacity, which is superior to most of the reported aerogels such as Al-L1 aerogel, Na-MnOx aerogel, and SiN-rGO aerogel [23–25]. Furthermore, as shown in Fig. 6A, all these four phenolic resin-based aerogels exhibited satisfied SO_2 adsorption rates with an equilibrium time of less than 5 min. AG-0.15 nanofiber aerogel achieved an SO_2 adsorption capacity of 9.16 mmol g^{-1} at a short time of 3.1 min, which is much better than many benchmark porous materials, including zeolites [8], porous carbon [34], MOFs [35], and covalent organic polymers [36].

Table 1
The adsorption capacities of SO_2 and CO_2 on four phenolic resin-based aerogels and other adsorbents at 1.0 bar.

Samples	SO_2(mmol g^{-1})		CO_2(mmol g^{-1})	Temperature (K)	Ref.
	0.01 bar	1.0 bar	1.0 bar		
AG-0.15 aerogel	1.43	10.58	0.21	298.2	This work
AG-0.10 aerogel	0.74	8.39	0.33	298.2	This work
AG-0.05 aerogel	0.64	7.41	0.36	298.2	This work
AG-0.00 aerogel	0.19	4.98	0.62	298.2	This work
Cr-L1 aerogel	0.68	4.8	1.0	293.2	[23]
AlCr-L1 aerogel	0.70	4.7	1.2	293.2	[23]
Al-L1 aerogel	0.52	6.6	0.8	293.2	[23]
H-MnO_x aerogel	–	0.6	–	293.2	[24]
Na-MnO_x aerogel	–	0.9	–	293.2	[24]
SiN-rGO aerogel	–	2.19	0.33	298.2	[25]
rGO aerogel	–	1.61	0.25	298.2	[25]

The effect of temperature on the adsorption of SO_2 by AG-0.15 nanofiber aerogel was also investigated, as shown in Fig. 6B. It can be seen that the adsorption capacity of SO_2 decreased with the increase of temperature, showing an exothermic adsorption process. Nevertheless, AG-0.15 nanofiber aerogel retained a considerable adsorption capacity of ~ 5 mmol g^{-1} even at a high temperature of 338.2 K. This suggests that the AG −0.15 aerogel has a good potential for SO_2 capture at high temperature. Furthermore, the isosteric heats for the capture of SO_2 by AG-0.15 nanofiber aerogel were calculated to be − 22 to − 14 kJ mol^{-1} based on the relationship between SO_2 uptake performance and temperature, (Fig. 6C), verifying the physical interaction between AG-0.15 and SO_2. In addition, the adsorption capacities of N_2 and CO_2 on AG-0.15 nanofiber aerogel were further determined to evaluate the adsorption selectivity of SO_2/N_2 and SO_2/CO_2. As shown in Fig. 6D, AG-0.15 nanofiber aerogel showed very low N_2 and CO_2 adsorption capacities of 0.003 and 0.21 mmol g^{-1} at 298.2 K and 1.0 bar. Accordingly, the IAST selectivities of SO_2/N_2 and SO_2/CO_2 were calculated to be 7271 for SO_2/N_2 (10/90 mixture) and 120 for SO_2/CO_2 (10/90 mixture), respectively. Howerve, it is showed that the selectivities of SO_2/N_2 and SO_2/CO_2 on AG-0.10, AG-0.05, and AG-0.00 aerogels were significantly lower than that of AG-0.15 (Table S1, Supplementary data). Therefore, AG-0.15 nanofiber aerogel has a good potential for selective adsorption and separation of SO_2 from flue gas containing CO_2 and N_2.

3.3. Dynamic breakthrough performance

To examine the actual SO_2/CO_2 and SO_2/N_2 separation capability on AG-0.15 nanofiber aerogel, a breakthrough test was performed using a simulated flue gas mixture ($SO_2/CO_2/N_2$) including 2000 ppm SO_2 with a flow rate of 20 mL min^{-1} at 298.2 K and 1.0 bar (Fig. 7). It is found that the breakthrough of SO_2 on AG-0.15 nanofiber aerogel was very slow and the retention time reached up to 450 min g^{-1}. For the competitive gases N_2 and CO_2, the breakthrough of 84.8% N_2 and 15% CO_2 rapidly eluted from the column bed. More importantly, as the result of good SO_2 uptake performance at high temperature, a breakthrough experiment for 2000 ppm SO_2 capture was performed at 338.2 K (Fig. S5, Supplementary data). It is showed that the breakthrough time of SO_2 on AG-0.15 nanofiber aerogel still reached as long as 45 min g^{-1} even at 338.2 K. This finding reconfirms the potential application of AG-0.15 nanofiber aerogel for SO_2 adsorption in actual flue gas at high temperature.

3.4. SO_2 adsorption mechanism

To gain an insight into good SO_2 adsorption capacity and SO_2/CO_2 selectivity, the mechanism in the adsorption of SO_2 by AG-0.15

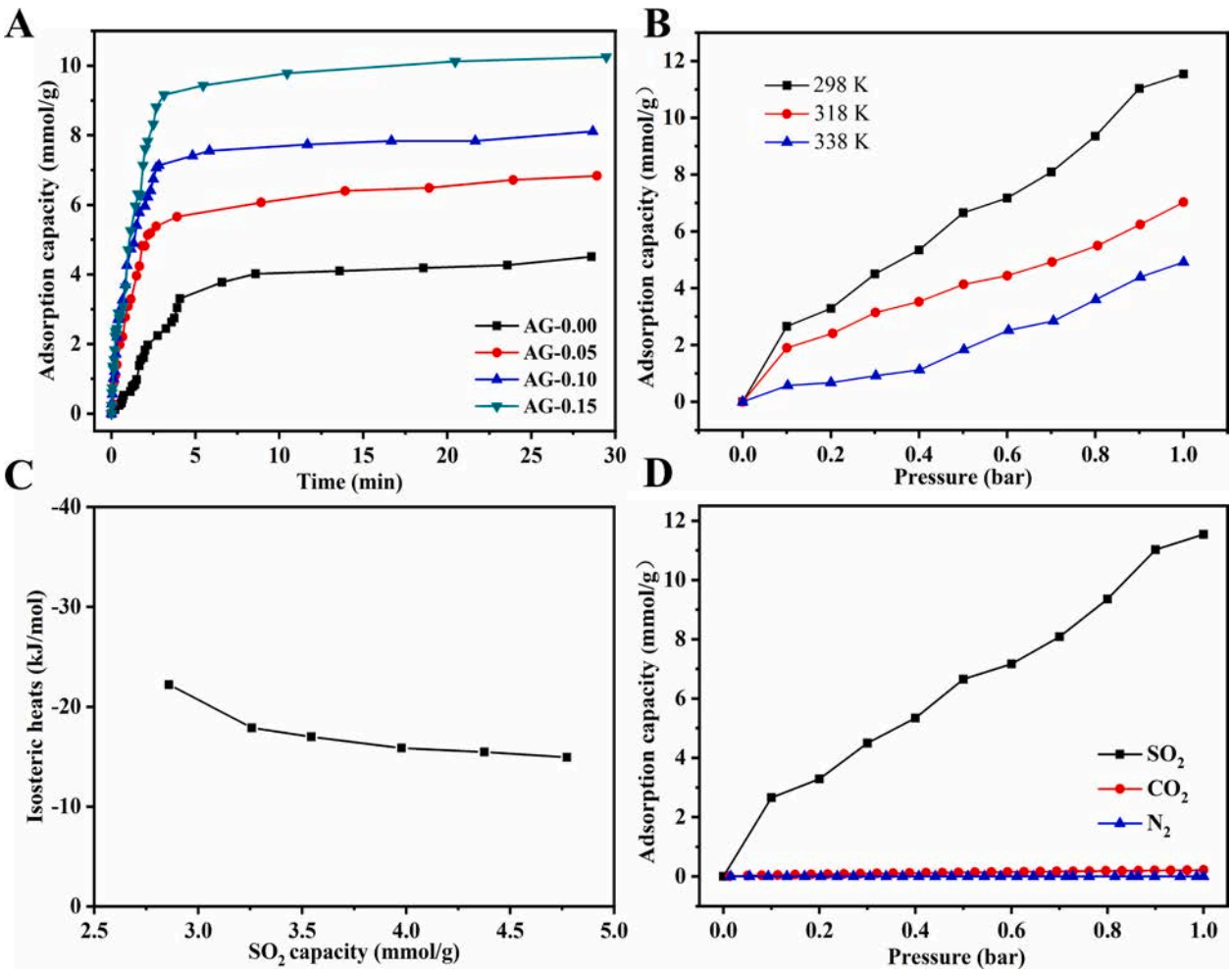

Fig. 6. SO_2 adsorption rate of four phenolic resin-based aerogels (A), the effect of temperature on SO_2 uptake by AG-0.15 (B), the isosteric heats of SO_2 adsorption on AG-0.15 (C), and SO_2, CO_2, and N_2 adsorption isotherms of AG-0.15 at 298.2 K and 1.0 bar (D).

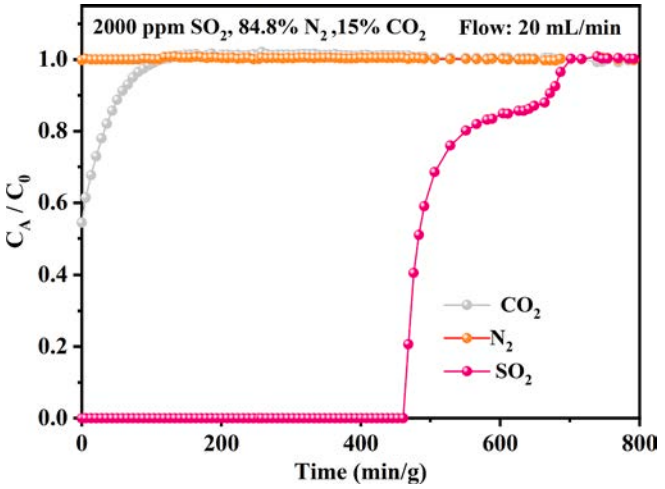

Fig. 7. Experimental column breakthrough curves for simulated flue gas compositions with AG-0.15 adsorbent at 298.2 K and 1.0 bar.

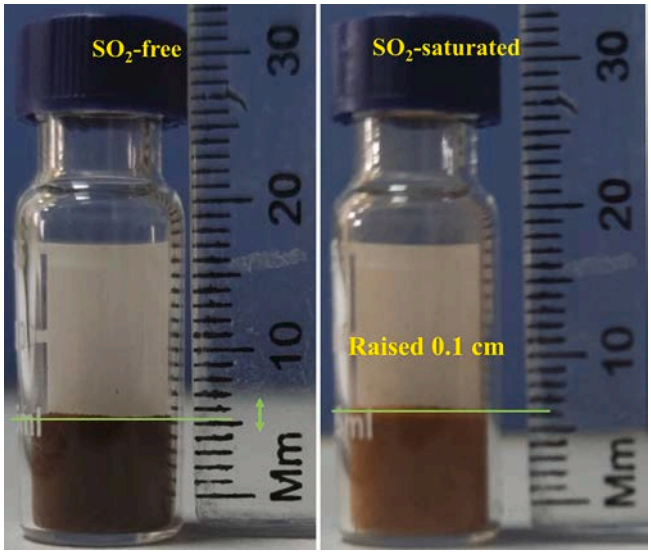

Fig. 8. The observable volume changes in AG-0.15 nanofiber aerogel before and after SO_2 adsorption.

nanofiber aerogel was explored. Firstly, the appearance volume changes in AG-0.15 nanofiber aerogel before and after SO_2 adsorption were shown in Fig. 8. It is found that the color of AG-0.15 nanofiber aerogel changed from a deep yellow to a pale yellow, and the volume of SO_2-saturated AG-0.15 nanofiber aerogel improved obviously compared

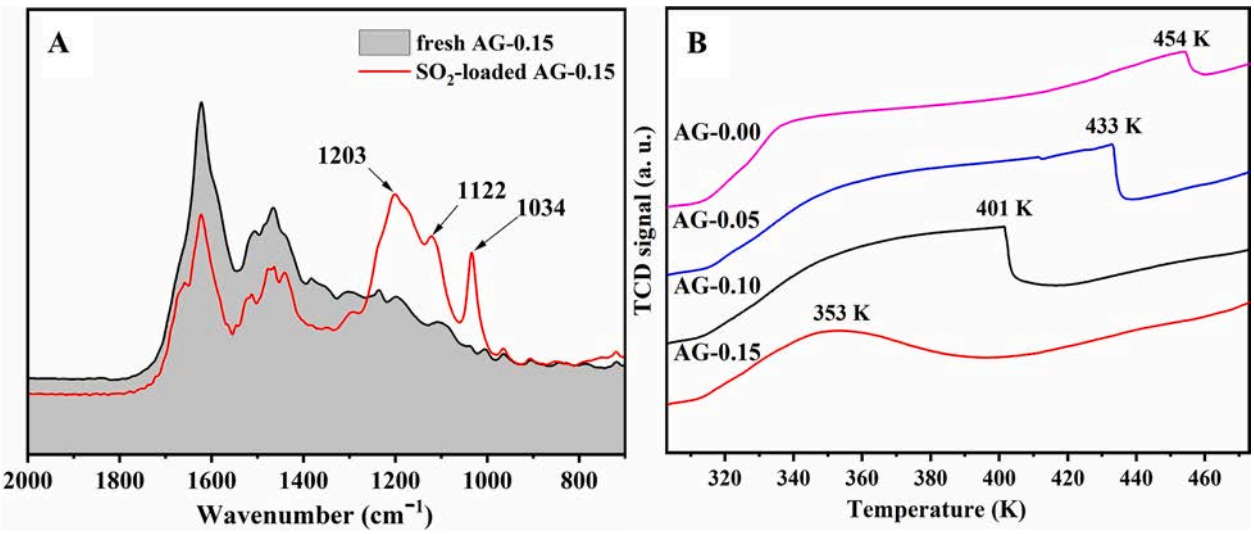

Fig. 9. FTIR spectra of fresh and SO_2-loaded AG-0.15 nanofiber aerogel (A) and TPD-CO_2 profiles of four phenolic resin-based aerogels (B).

with that of fresh AG-0.15 nanofiber aerogel. This finding suggests that SO_2 molecular has been successfully entered into AG-0.15 nanofiber aerogel through a swelling mechanism, which is well in agreement with the previous result reported by Xing et al [37,38]. Moreover, Fig. 9A shows the FTIR spectra of AG-0.15 nanofiber aerogel before and after SO_2 adsorption. It can be seen that three new peaks at 1203, 1122, and 1034 cm^{-1} were observed after AG-0.15 nanofiber aerogel capturing SO_2. The peaks at 1203 and 1122 cm^{-1} can be attributed to the asymmetrical and symmetric stretching vibrations of S = O, respectively [39,40]. The peak at 1034 cm^{-1} is attributed to the π•••S interaction between the phenyl group in AG-0.15 and S in SO_2 [14]. Compared to fresh SO_2 (1145 cm^{-1} for the symmetrical stretch of S = O) [39], the vibrational frequency of adsorbed SO_2 on AG-0.15 nanofiber aerogel was slightly red-shifted, implying that AG-0.15 nanofiber aerogel does not interact with SO_2 strongly and the adsorbed SO_2 would be easily desorbed and released during the desorption procedure. This finding is consistent with the observation of XPS analysis of tertiary N in AG-0.15 nanofiber aerogel.

In addition, the interaction between phenolic resin-based aerogels and CO_2 was further studied by CO_2-TPD to explain the highest selectivity of SO_2/CO_2 in AG-0.15 nanofiber aerogel. As shown in Fig. 9B, these four phenolic resin-based aerogels exhibited different desorption temperatures of CO_2, and the sequence was AG-0.00 > AG-0.05 > AG-0.10 > AG-0.15. Notably, AG-0.15 nanofiber aerogel possessed the lowest desorption temperature of CO_2 at 353 K, implying the weakest interaction between AG-0.15 and CO_2. As a result, AG-0.15 nanofiber aerogel would lead to the lowest CO_2 uptake capacity than the other three aerogels, which is consistent with the sequence of CO_2 adsorption performance of four phenolic resin-based aerogels in Table 1. Therefore, AG-0.15 nanofiber aerogel exhibited excellent SO_2 uptake and very low CO_2 uptake, resulting in the best SO_2/CO_2 selectivity.

3.5. Recycling test of AG-0.15

As shown in Fig. 10, the SO_2 adsorption performance on AG-0.15 nanofiber aerogel was not observed to decline during eight adsorption–desorption cycles. This shows that AG-0.15 nanofiber aerogel has outstanding reversibility for the adsorption of SO_2. The FTIR spectra of recycled AG-0.15 nanofiber aerogel are almost the same as that of the fresh sample, as shown in Fig. S6 in the Supplementary data. It is found that the FTIR spectra of regenerated AG-0.15 nanofiber aerogel were nearly the same as the fresh sample during 8-cycle runs, showing the good stability of AG-0.15 nanofiber aerogel. Also, SO_2 could be completely desorbed from AG-0.15 nanofiber aerogel, reconfirming that the physical SO_2 adsorption process is highly reversible.

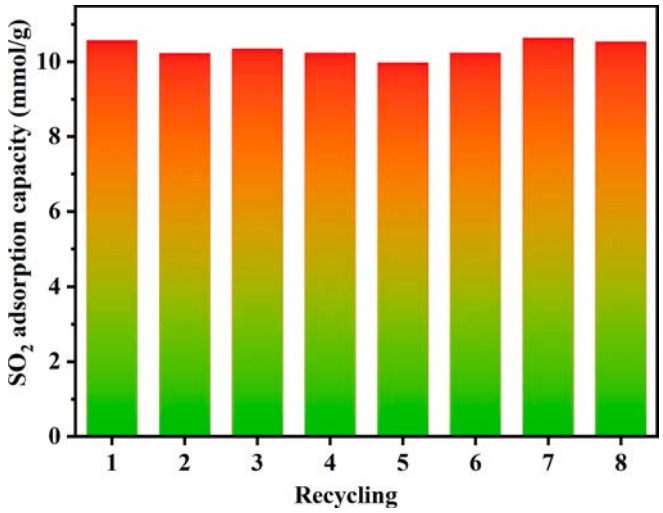

Fig. 10. Recycle performance of AG-0.15 for SO_2 adsorption at 298.2 K and 1.0 bar.

4. Conclusions

In summary, four phenolic resin-based aerogels with controlled structures and morphologies were synthesized, characterized, and used as excellent adsorbents for SO_2 separation. It is demonstrated that adjusting the usage amount of CTAB from 0.00 to 0.15 g could effectively regulate the morphology and size of phenolic resin-based aerogels varying from spherical (~1 μm) to nanofiber (~20 nm). AG-0.15 nanofiber aerogel had the best SO_2 uptake capacity of 10.58 mmol g^{-1} at 298.2 K and 1.0 bar, as well as the highest selectivity of SO_2/N_2 selectivity was up to 7271 (i.e., 10/90 mixture at 298.2 K and 1 bar). Moreover, the outstanding separation performance in deeply removing 2000 ppm SO_2 on AG-0.15 nanofiber aerogel was further confirmed by dynamic column breakthrough experiments with the mixture of $SO_2/N_2/CO_2$. In addition, AG-0.15 nanofiber aerogel showed good enough reversibility and recyclability for eight SO_2 adsorption/desorption cycles. This work illustrates that using CATB as a soft template for the synthesis of high-performance phenolic resin aerogel is a successful strategy for achieving efficient, selective, and reversible SO_2 capture.

Declaration of Competing Interest

The authors declare that they have no known competing financial interests or personal relationships that could have appeared to influence the work reported in this paper.

Acknowledgments

This work was supported by the National Natural Science Foundations of China (22068013), the Natural Science Foundations of Jiangxi Province (20192ACBL20025), the Key Research and Development Program of Jiangxi Province (20202BBGL73118), and the Science and Technology Research Program of Jiangxi Provincial Education Department (GJJ200339) for financial support.

References

[1] E. Martínez-Ahumada, D. He, V. Berryman, A. López-Olvera, M. Hernandez, V. Jancik, V. Martis, M.A. Vera, E. Lima, D.J. Parker, A.I. Cooper, I.A. Ibarra, M. Liu, SO_2 capture using porous organic cages, Angew. Chem. Int. Ed. 60 (32) (2021) 17556–17563.

[2] H.C. Lan, Y.T. Zou, Y.C. Wang, N.N. Cheng, W.L. Xu, H.L. Peng, K. Huang, L. Y. Kong, J. Du, Enhancing the activity of MoS_2/SiO_2-Al_2O_3 bifunctional catalysts for suspended-bed hydrocracking of heavy oils by doping with Zr atoms, Chinese J. Chem. Eng. (2021), https://doi.org/10.1016/j.cjche.2021.03.015.

[3] H.C. Lan, Y.T. Zou, Y.C. Wang, N.N. Cheng, W.L. Xu, H.L. Peng, K. Huang, L. Y. Kong, J. Du, Meso-macroporous polymer densely functionalized with tertiary amine groups as effective sorbents for SO_2 capture, Chem. Eng. J. 442 (2021), 129699.

[4] H.C. Lan, Y.J. Zhang, Q.J. Dai, H. Ye, X.Y. Mao, Y.C. Wang, H.L. Peng, J. Du, K. Huang, Highly efficient, selective and reversible capture of sulfur dioxide by methylated-polyethylenimine supported on graphitic carbon nitride, Chem. Eng. J. 409 (2021), 127378.

[5] S. Popa, B. Ungureanu, I. Gheonea, A. Mitrea, C. Ardeleanu, M. Ghilusi, V. Surlin, E. Georgescu, I. Georgescu, M. Mota, O.M. Marioara, A. Saftoiu, Pitfalls in diagnosing a pancreatic neuroendocrine tumor: a case report, Rom. J. Morphol. Embryol. 56 (2015) 1495–1502.

[6] P. Córdoba, Status of Flue Gas Desulphurisation (FGD) systems from coal-fired power plants: Overview of the physic-chemical control processes of wet limestone FGDs, Fuel 144 (2015) 274–286.

[7] Z. Yan, S. Tang, X. Zhou, L.i. Yang, X. Xiao, H. Chen, Y. Qin, W. Sun, All-silica zeolites screening for capture of toxic gases from molecular simulation, Chinese, J Chem. Eng. 27 (1) (2019) 174–181.

[8] H. Deng, H. Yi, X. Tang, Q. Yu, P. Ning, L. Yang, Adsorption equilibrium for sulfur dioxide, nitric oxide, carbon dioxide, nitrogen on 13X and 5A zeolites, Chem. Eng. J. 188 (2012) 77–85.

[9] Y.L. Fan, H.P. Zhang, M.J. Yin, R. Krishna, X.F. Feng, L.i. Wang, M.B. Luo, F. Luo, High adsorption capacity and selectivity of SO_2 over CO_2 in a metal-organic framework, Inorg. Chem. 60 (1) (2021) 4–8.

[10] J.Y. Zhang, J.B. Zhang, M. Li, Z. Wu, S. Dai, K. Huang, Solvent-free and one-pot synthesis of ultramicroporous carbons with ultrahigh nitrogen contents for sulfur dioxide capture, Chem. Eng. J. 391 (2020), 123579.

[11] W. Kong, Y. Liu, J. Liu, Design of highly nitrogen-doped, two-dimensional hierarchical porous carbons with superior performance for selective capture of CO_2 and SO_2, Energ, Fuel. 34 (3) (2020) 3557–3565.

[12] H. Wang, X. Zeng, W. Wang, D. Cao, Selective capture of trace sulfur gas by porous covalent-organic materials, Chem. Eng. Sci. 135 (2015) 373–380.

[13] J.H. Carter, X. Han, F.Y. Moreau, I. da Silva, A. Nevin, H.G.W. Godfrey, C.C. Tang, S. Yang, M. Schröder, Exceptional adsorption and binding of sulfur dioxide in a robust zirconium-based metal–organic framework, J. Am. Chem. Soc. 140 (46) (2018) 15564–15567.

[14] X.C. An, Z.M. Li, Y. Zhou, W. Zhu, D.J. Tao, Rapid capture and efficient removal of low-concentration SO_2 in simulated flue gas by hypercrosslinked hollow nanotube ionic polymers, Chem. Eng. J. 394 (2020), 124859.

[15] Y. Kong, X. Shen, S. Cui, M. Fan, Development of monolithic adsorbent via polymeric sol–gel process for low-concentration CO_2 capture, Appl. Energ. 147 (2015) 308–317.

[16] C. Chen, S. Zhang, K.H. Row, W.-S. Ahn, Amine–silica composites for CO_2 capture: A short review, J. Energy Chem. 26 (5) (2017) 868–880.

[17] N. Minju, P. Abhilash, B.N. Nair, A.P. Mohamed, S. Ananthakumar, Amine impregnated porous silica gel sorbents synthesized from water–glass precursors for CO_2 capturing, Chem. Eng. J. 269 (2015) 335–342.

[18] W. Wang, J. Motuzas, X.S. Zhao, J.C. Diniz da Costa, 2D/3D assemblies of amine-functionalized graphene silica (templated) aerogel for enhanced CO_2 sorption, ACS Appl. Mater. Inter. 11 (33) (2019) 30391–30400.

[19] Y. Li, P. Jia, J. Xu, Y.u. Wu, H. Jiang, Z. Li, The aminosilane functionalization of cellulose nanofibrils and the mechanical and CO_2 adsorption characteristics of their aerogel, Ind. Eng. Chem. Res. 59 (7) (2020) 2874–2882.

[20] L. Keshavarz, M.R. Ghaani, J.M.D. MacElroy, N.J. English, A comprehensive review on the application of aerogels in CO_2-adsorption: Materials and characterisation, Chem. Eng. J. 412 (2021), 128604.

[21] J.-H. Lee, S.-J. Park, Recent advances in preparations and applications of carbon aerogels: A review, Carbon 163 (2020) 1–18.

[22] A.M. ElKhatat, S.A. Al-Muhtaseb, Advances in tailoring resorcinol-formaldehyde organic and carbon gels, Adv. Mater. 23 (26) (2011) 2887–2903.

[23] D. Dietrich, C. Licht, A. Nuhnen, S.-P. Höfert, L. De Laporte, C. Janiak, Metal-organic gels based on a bisamide tetracarboxyl ligand for carbon dioxide, sulfur dioxide, and selective dye uptake, ACS Appl. Mater. Inter. 11 (21) (2019) 19654–19667.

[24] J.W. Long, J.M. Wallace, G.W. Peterson, K. Huynh, Manganese oxide nanoarchitectures as broad-spectrum sorbents for toxic gases, ACS Appl. Mater. Inter. 8 (2) (2016) 1184–1193.

[25] S. Yun, H. Kim, H. Lee, H.S. Park, Three-dimensionally macroporous, Si and N-incorporated graphene aerogels for gas adsorbents, Mater. Express 5 (5) (2015) 463–469.

[26] F.F. Chen, K. Huang, J.P. Fan, D.J. Tao, Chemical solvent in chemical solvent: A class of hybrid materials for effective capture of CO_2, AIChE J. 64 (2018) 632–639.

[27] F.-F. Chen, K. Huang, Y. Zhou, Z.-Q. Tian, X. Zhu, D.-J. Tao, D.-e. Jiang, S. Dai, Multi-molar absorption of CO_2 by the activation of carboxylate groups in amino acid ionic liquids, Angew. Chem. Int. Ed. 55 (25) (2016) 7166–7170.

[28] A.L. Myers, P.A. Monson, Adsorption in porous materials at high pressure: theory and experiment, Langmuir 18 (2002) 10261–10273.

[29] F.R. Siperstein, A.L. Myers, Mixed-gas adsorption, AIChE J. 47 (5) (2001) 1141–1159.

[30] L. Yan, Y. Cui, G. Gou, Q.i. Wang, M. Jiang, S. Zhang, D. Hui, J. Gou, Z. Zhou, Liquefaction of lignin in hot-compressed water to phenolic feedstock for the synthesis of phenol-formaldehyde resins, Compos. Part B-Eng. 112 (2017) 8–14.

[31] Y.u. Chen, H.-B. Zhang, M.u. Wang, X. Qian, A. Dasari, Z.-Z. Yu, Phenolic resin-enhanced three-dimensional graphene aerogels and their epoxy nanocomposites with high mechanical and electromagnetic interference shielding performances, Compos. Sci. Technol. 152 (2017) 254–262.

[32] W. Luo, T. Zhao, Y. Li, J. Wei, P. Xu, X. Li, Y. Wang, W. Zhang, A.A. Elzatahry, A. Alghamdi, Y. Deng, L. Wang, W. Jiang, Y. Liu, B. Kong, D. Zhao, A micelle fusion–aggregation assembly approach to mesoporous carbon materials with rich active sites for ultrasensitive ammonia sensing, J. Am. Chem. Soc. 138 (38) (2016) 12586–12595.

[33] J. Li, D. Jia, Z. Guo, Y. Liu, Y. Lyu, Y.u. Zhou, J. Wang, Imidazolinium based porous hypercrosslinked ionic polymers for efficient CO_2 capture and fixation with epoxides, Green Chem. 19 (11) (2017) 2675–2686.

[34] A. Wang, R. Fan, X. Pi, S. Hao, X. Zheng, Y. Yang, N-Doped porous carbon derived by direct carbonization of metal–organic complexes crystal materials for SO_2 adsorption, Cryst. Growth Des. 19 (3) (2019) 1973–1984.

[35] L. Li, I. da Silva, D.I. Kolokolov, X. Han, J. Li, G. Smith, Y. Cheng, L.L. Daemen, C. G. Morris, H.G.W. Godfrey, N.M. Jacques, X. Zhang, P. Manuel, M.D. Frogley, C. A. Murray, A.J. Ramirez-Cuesta, G. Cinque, C.C. Tang, A.G. Stepanov, S. Yang, M. Schroder, Post-synthetic modulation of the charge distribution in a metal–organic framework for optimal binding of carbon dioxide and sulfur dioxide, Chem. Sci. 10 (5) (2019) 1472–1482.

[36] Y.u. Fu, Z. Wang, S. Li, X. He, C. Pan, J. Yan, G. Yu, Functionalized covalent triazine frameworks for effective CO_2 and SO_2 removal, ACS Appl. Mater. Inter. 10 (42) (2018) 36002–36009.

[37] L. Xia, Q. Cui, X. Suo, Y.H. Li, X.L. Cui, Q.W. Yang, J.H. Xu, Y.W. Yang, H.B. Xing, Efficient, selective, and reversible SO_2 capture with highly crosslinked ionic microgels via a selective swelling mechanism, Adv. Funct. Mater. 28 (2018) 1704292.

[38] X. Suo, Y. Yu, S. Qian, L. Zhou, X. Cui, H. Xing, Tailoring the pore size and chemistry of ionic ultramicroporous polymers for trace sulfur dioxide capture with high capacity and selectivity, Angew. Chem. Int. Ed. 60 (13) (2021) 6986–6991.

[39] D. Yang, S. Zhang, D.-e. Jiang, S. Dai, SO_2 absorption in EmimCl-TEG deep eutectic solvents, Phys. Chem. Chem. Phys. 20 (22) (2018) 15168–15173.

[40] Y. Wang, W. Zhao, M. Chai, G. Li, Q. Jia, Y. Chen, Phase-change absorption of SO_2 by imidazole in organic solvents and conversion of the absorption product in the presence of water and oxygen, Energ, Fuel. 31 (12) (2017) 13999–14006.